ACS APPLIED MATERIALS & INTERFACES

Research Article

www.acsami.org

Switching Transport through Nanopores with pH-Responsive Polymer Brushes for Controlled Ion Permeability

G. Wilhelmina de Groot,[†] M. Gabriella Santonicola,[†,▽] Kaori Sugihara,[‡,#] Tomaso Zambelli,[‡] Erik Reimhult,[§] János Vörös,[‡] and G. Julius Vancso*[,†]

[†]Materials Science and Technology of Polymers, MESA+ Institute for Nanotechnology, University of Twente, P.O. Box 217, 7500 AE Enschede, The Netherlands

[‡]Laboratory of Biosensors and Bioelectronics, Institute for Biomedical Engineering, ETH Zürich, Gloriastrasse 35, 8092 Zürich, Switzerland

[§]Institute for Biologically Inspired Materials, Department of Nanobiotechnology, University of Natural Resources and Life Sciences Vienna, Muthgasse 11, 1190 Vienna, Austria

Supporting Information

ABSTRACT: Several nanoporous platforms were functionalized with pH-responsive poly(methacrylic acid) (PMAA) brushes using surface-initiated atom transfer radical polymerization (SI-ATRP). The growth of the PMAA brush and its pH-responsive behavior from the nanoporous platforms were confirmed by scanning electron microscopy (SEM), Fourier transform infrared (FTIR) spectroscopy, and atomic force microscopy (AFM). The swelling behavior of the pH-responsive PMAA brushes grafted only from the nanopore walls was investigated by AFM in aqueous liquid environment with pH values of 4 and 8. AFM images displayed open nanopores at pH 4 and closed ones at pH 8, which rationalizes their use as gating platforms. Ion conductivity across the nanopores was investigated with current−voltage measurements at various pH values. Enhanced higher resistance across the nanopores was observed in a neutral polymer brush state (lower pH values) and lower resistance when the brush was charged (higher pH values). By adding a fluorescent dye in an environment of pH 4 or pH 8 at one side of the PMAA-brush functionalized nanopore array chips, diffusion across the nanopores was followed. These experiments displayed faster diffusion rates of the fluorescent molecules at pH 4 (PMAA neutral state, open pores) and slower diffusion at pH 8 (PMAA charged state, closed pores) showing the potential of this technology toward nanoscale valve applications.

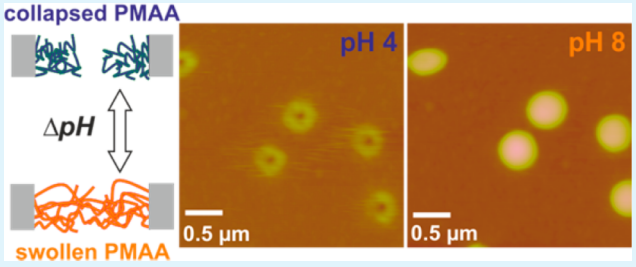

KEYWORDS: *pH-responsive polymer brushes, poly(methacrylic acid), grafting from surfaces, atomic force microscopy, nanopores, ion gating*

1. INTRODUCTION

Functionalization of porous platforms with stimulus-responsive polymer brush structures allows reversible controlled switching of surface properties inside microchannels and nanochannels, and makes it possible to fabricate valves at these length scales. These functionalized porous platforms can be applied in biosensing, where they can provide stable devices to increase mechanical stability and lifetime for membrane protein screening.[1]

Stimulus-responsive polymer grafts have been used with great success to engineer the surfaces of materials. The switching can be triggered by an external stimulus in the environment of the material, e.g., changes in pH, temperature, mechanical force, or light.[2] Surface-initiated controlled radical polymerization techniques are mostly used to synthesize these polymer brush structures, and the technique used most frequently is surface-initiated atom transfer radical polymerization (SI-ATRP).[3] SI-ATRP provides an environment in which polymer brush growth is reproducible and yields robust polymer brush structures, well-defined in chain length and architecture. Grafting density can, in principle, be controlled by tuning the coverage of initiators attached to the substrates.[4−7]

Grafting stimulus-responsive polymer brushes via SI-ATRP from porous platforms offers opportunities to different fields including delivery systems, lab-on-a-chip, microfluidics and nanofluidics, and (bio)molecular screening.[8] Weak polyelectrolyte brushes are especially interesting, because they make it possible to control ion permeation through porous platforms by varying the pH of the surrounding solution,[9−11] and they can be useful in their swollen state as an alternative approach to support and span lipid bilayers over pores.[12−17] Both of these functionalities open ways to incorporate membrane proteins in

Received: November 23, 2012
Accepted: January 29, 2013
Published: January 29, 2013

ACS Publications © 2013 American Chemical Society

dx.doi.org/10.1021/am302820y | ACS Appl. Mater. Interfaces 2013, 5, 1400−1407

the supported lipid bilayer and measure their ion channel activity for pharmaceutical relevance.[18,19] This approach can create functional sensor surfaces with immobilized membrane proteins that are suitable for in-vitro-controlled electrochemical recording of their structural−functional relationships and for label-free high-throughput screening of low-molecular-weight drug candidates. Another interesting possibility is the coupling of nitrilotriacetate (NTA) to polymer brushes with carboxylic acid groups via EDC/NHS activation for precise positioning of membrane proteins above the pore openings of the platforms.[20,21]

Control of transport through polymeric membranes functionalized with smart polymer systems has already been described for both responsive polymer brush structures and (grafted) responsive hydrogels.[22,23] It has been displayed that permeation of water and polymer solution through polymer brush functionalized polymeric membranes can be controlled by changing the pH of the surrounding environment.[24−26] Besides pH-responsive polymer brush structures, thermo-responsive polymer brushes were also grafted to and from track-etched membranes. *N*-isopropylacrylamide (NIPAM) was polymerized by controlled radical polymerization techniques, and the functionalized membranes were characterized with conductometric measurements below and above the lower critical solution temperature of poly-NIPAM (PNIPAM), resulting in different permeabilities.[27,28] More recently, pH-responsive polymer brush structures were grafted from single polymeric nanopores. Functionalized nanopores displayed a variation in transport of protons across the single-pore membranes, in response to a change in pH. This pH-responsive behavior originated from the protonation below pH 5 of the pyridine groups in the poly(4-vinyl pyridine) (PVP) brush, which resulted in a charged and swollen brush. In particular, current−voltage measurements showed that, above pH 5 (neutral brush), the ionic conductance was constant and low, compared to pH values below pH 5 (charged brush), where the ionic conductance increased.[29] The functionalization of macro-porous silicon membranes with weak polyelectrolyte brushes synthesized by SI-ATRP was reported by the same group. These weak polyelectrolyte brush functionalized membranes were mainly characterized with a focus on proton conductivity for fuel cell applications.[30,31]

The examples mentioned above demonstrate that current−voltage measurements are a convenient tool for investigating the ionic conductance of membranes functionalized with weak polyelectrolyte brushes in combination with pH variations. In addition, it is also reported that resistance measurements can be performed at polyelectrolyte multilayer filled nanopores,[32] which is used for measuring the resistance of supported lipid bilayers spanned over these functionalized pores.[12] Atomic force microscopy (AFM) is a well-known characterization technique for polymer brush structures, and applying AFM in a liquid environment makes it possible to monitor the responsive behavior on the polymer brush.[33−36] The influence of the force applied by a AFM tip was investigated by force volume spectroscopy for polyethylene glycol chains anchored to a nanoring on a substrate. Applying less or more force changed the AFM image, because of the indentation of the AFM tip in the polymer brush structure.[37] Yet another useful characterization method is fluorescence spectroscopy, which makes it possible to follow the transport of fluorescent molecules from one side to the other of the membrane.[38]

Previously, we reported fast and reversible switching between polymer conformations at low and high pH values for pH-responsive poly(methacrylic acid) (PMAA) brushes grafted from planar silicon surfaces. In that study, the methanol content of the aqueous ATRP reaction mixture was varied to investigate further applications for controlled brush growth in confined spaces.[10]

Here, we apply the brush growth from our previous study to several nanoporous platforms and characterize the polymerization using different techniques displaying the growth of PMAA brushes inside the nanopores. Current−voltage measurements, and diffusion experiments in combination with fluorescence spectroscopy, demonstrate control of transport through the functionalized pores by variations in the pH of the surrounding environment.

2. EXPERIMENTAL SECTION

2.1. Materials. Allyl 2-bromo-2-methylpropionate (CAS No. 40630-82-8, 98%), chlorodimethylhydrosilane (CAS No. 1066-35-9, 98%), chloroplatinic acid hexahydrate (CAS No. 18497-13-7, ≥ 37.50% Pt basis), sodium methacrylate (CAS No. 5536-61-8, 99%), CuBr (CAS No. 7787-70-4, 99.999%), $CuBr_2$ (CAS No. 7789-45-9, 99.999%), 2,2′-bipyridine (CAS No. 366-18-7, ≥99.0%), Rhodamine 6G (CAS No. 989-38-8, dye content ∼95%) were purchased from Sigma−Aldrich and used without further purification. All solvents were of high purity, and deionized water from a Milli-Q purification system (Millipore Advantage A10) was used throughout. Phosphate solutions (50 mM phosphate) with various pH values were prepared by titrating aliquots from the same stock (pH 7.4), using HCl or KOH solutions.

Nanoporous silicon nitride films with pore diameters of 200 nm and a pore depth of 300 nm were prepared by colleagues of the Laboratory for Surface Science and Technology at ETH Zürich, using particle lithography.[39,40] The nanopores were etched in silicon nitride films supported on silicon or glass substrates; these will be referenced hereafter as nanowells. Such nanoporous films were used with or without a passivating chrome layer on the top surface. Chips with a single pore or with an array of pores accessible on both sides in a 5 mm × 5 mm and 300-nm-thick silicon nitride membrane were fabricated by Leister Technologies AG.[41] Chips with 4 pores 400 nm in diameter, 1 pore 800 nm in diameter, and 512 pores 800 nm in diameter were used. The pores of these chips will be indicated as nanochannels in the rest of this work.

2.2. Nanopore Functionalization with PMAA Brushes. All nanoporous platforms were functionalized combining ATRP and the grafting from approach following a previously published procedure.[10] Briefly, nanoporous silicon nitride surfaces were cleaned and activated in piranha solution (H_2SO_4/H_2O_2 70:30 v/v) for 30 min, rinsed with water and ethanol, and dried in a stream of nitrogen. *[**Warning: Piranha solution reacts strongly with organic compounds and should be handled with extreme caution.**]* Next, a monolayer of the ATRP initiator (3-(2-bromoisobutyryl)propyl)dimethylchlorosilane was deposited on the nanoporous surfaces by vapor phase deposition, which was followed by ATRP of sodium methacrylate at room temperature for 1 h under an argon atmosphere. The surface-initiated ATRP was performed in a water/methanol mixture 50:50 v/v to improve the wetting of the pore walls and allow for polymer brush growth inside the nanopores. Sodium methacrylate (50 mmol) was dissolved in the ATRP medium (10 mL) and the solution degassed before

addition to the Schlenk flask with CuBr (1 mmol), $CuBr_2$ (0.1 mmol), and 2,2′-bipyridine (2.2 mmol) under inert atmosphere. After stirring for 15 min, the ATRP mixture was transferred to the argon-filled vials with the initiator-coated nanoporous samples. After polymerization, the nanoporous chips were washed with water and with EDTA solution (0.1 M, pH 7), and then immersed in water overnight to remove any physisorbed polymer. Finally, chips were rinsed with ethanol and dried under nitrogen gas.

2.3. Characterization Techniques. *Scanning Electron Microscopy (SEM).* SEM images were taken with a HR-LEO Model 1550 FEF SEM system under vacuum. Cross sections of the nanoporous films were obtained by breaking the substrates after cleaning, in case of a nonfunctionalized nanoporous film, or after polymerization, in case of PMAA-brush functionalized nanoporous films.

Fourier Transform Infrared (FTIR) Spectroscopy. FTIR spectra were obtained with a Biorad Model FTS-575C spectrometer equipped with a nitrogen-cooled cryogenic mercury telluride detector (spectral resolution of 4 cm^{-1}, 1024 scans). The background spectrum was obtained by recording the spectrum of a cleaned silicon nitride nanoporous film. The pH-responsive behavior of PMAA brushes grafted from silicon nitride nanoporous films was investigated by immersing the PMAA-brush functionalized nanoporous film in a phosphate solution of pH 4 or pH 8 for 15 min, rinsing it with ethanol, drying it under a nitrogen stream, and scanning via FTIR spectroscopy.

Contact Angle Measurements. Static contact angle measurements were performed with the sessile drop method, using an optical contact angle device equipped with an electronic syringe unit (OCA15, Dataphysics, Germany). Degassed Milli-Q water was used as the probe liquid. For each sample, three successive measurements were made.

X-ray Photoelectron Spectroscopy (XPS). XPS was used to evaluate the immobilization of initiator molecules on silicon surfaces and chrome surfaces. A 20-nm-thick layer of chrome was evaporated on a silicon wafer to serve as a model surface. XPS spectra were obtained on a Quantera XPS instrument (Physical Electronics), using a monochromatized Al Kα radiation (1486.6 eV) source with an X-ray beam diameter of 100 μm and an electron take-off angle of 45°, relative to the sample surface. The spectrometer resolution was 0.2 eV for the high-resolution element scans and 0.4 eV for the survey spectra. An Ar^+-ion beam neutralizer was not used, to avoid damage to the labile Br atom of the initiator molecule.

Atomic Force Microscopy (AFM). AFM images of nonfunctionalized and PMAA-brush functionalized nanoporous films with a chrome top layer were obtained under ambient conditions in tapping mode (TM-AFM) with a NanoScope III Multimode setup (Digital Instruments/Veeco−Bruker, Santa Barbara, CA, USA), using silicon cantilevers with resonance frequencies of 200−500 kHz (type PPP-NCH-W, Nanosensors, Wetzlar, Germany) and a EV-scanner (Digital Instruments/Veeco−Bruker). The swelling behavior of the PMAA brush upon pH variation was evaluated by in situ AFM in liquid environment using a NanoScope III Multimode setup equipped with a liquid cell. AFM measurements were carried out in contact mode (CM-AFM) (with minimal loading force of ∼10 nN using optimized feedback parameters) using commercially available V-shaped Si_3N_4 cantilevers (model NP, k = 0.58 N/m, Digital Instruments/Veeco−Bruker).

Electrochemical Measurements. Current−voltage measurements were performed with an Autolab PSTAT12 Instrument (Ecochemie, Utrecht, The Netherlands). Current−voltage curves were obtained between two Ag/AgCl electrodes purchased from Lot-Oriel AG (WPI reference electrode for EC-QCM Module QSP 020). Nanopore array chips were placed in a two-chamber setup, and the chambers were filled with phosphate solutions of various pH. During the measurements, the two-chamber setup was placed in a Faraday cage.

Fluorescence Spectroscopy. Diffusion experiments with nanopore array chips functionalized with PMAA brushes were performed in a two-chamber setup filled with phosphate solutions of pH 4 or pH 8. The fluorescent dye Rhodamine 6G was added at one side of the chip, and after 19.5 h or 16 h, a sample for fluorescence spectroscopy was taken. After rinsing the setup, the phosphate solution was switched to the other pH and Rhodamine 6G was again added to one side of the polymer-brush functionalized nanopore chip. The calibration was performed by measuring the fluorometer responses of known concentrations of Rhodamine 6G dye molecules in phosphate solutions of pH 4 or pH 8. Fluorescence spectroscopy was performed with a Perkin−Elmer spectrometer.

3. RESULTS AND DISCUSSION

3.1. Functionalization and Characterization of Nanoporous Platforms with pH-Responsive Poly(methacrylic acid) Brushes. Supported and free-standing nanoporous silicon nitride films were functionalized with pH-responsive PMAA brushes using SI-ATRP. First, the pre-activated chips were treated by vapor-phase deposition with an initiator layer of (3-(2-bromoisobutyryl)propyl)dimethylchlorosilane molecules. Then, SI-ATRP of sodium methacrylate was conducted to synthesize pH-responsive PMAA brushes. SI-ATRP was performed in a water/methanol 50:50 v/v reaction mixture, to improve the wetting of the pore walls for polymer-brush growth inside the pores. The polymerization was performed for 1 h at room temperature, which resulted in PMAA brushes with a dry thickness of ∼90 nm, as measured by ellipsometry on planar silicon surfaces in air.[10] After polymerization, a color change at the surface of the substrates was observed, which was an initial indication of the film modification with the PMAA brush layer.

SEM was used to compare bare nanoporous films with PMAA-brush functionalized nanoporous films, to confirm the presence of the polymeric layer inside the nanowells (Figure 1). SEM images were taken from the top surface and the cross section, with the samples imaged in a tilted position. The images of the top sides clearly display that there is a layer of polymeric material on the functionalized nanoporous film. The pore openings are smaller in diameter and the edges of the pore openings are much smoother. The cross-sectional SEM images confirm that (i) there is polymeric material inside the nanowells, and (ii) the added layer on the functionalized nanoporous film is ∼60 nm thick.

FTIR spectroscopy was used to confirm the pH-responsive behavior of the PMAA brush grafted from the nanoporous film. A functionalized nanoporous film was immersed in a phosphate solution of pH 4 or pH 8, and a FTIR spectrum was taken. Figure 2 displays the carbonyl absorption region of the PMAA brush immediately after immersion in each solution. The characteristic band peak of the protonated carboxylic acid groups is found at 1705 cm^{-1}, whereas the characteristic band

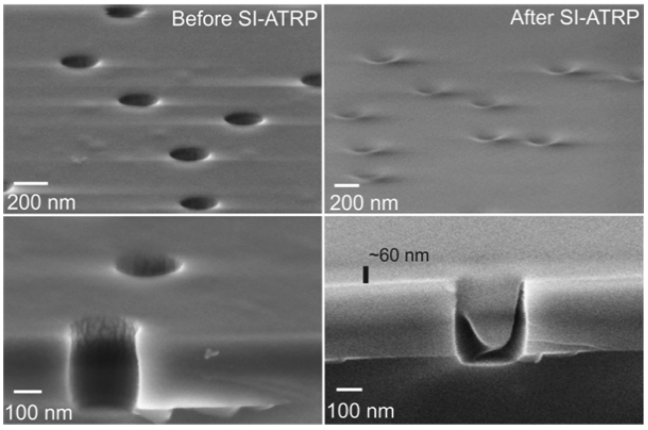

Figure 1. SEM images of nonfunctionalized (left) and PMAA-brush functionalized (right) nanoporous silicon nitride films without a chrome top layer. Top images display tilted top surface views and bottom images display cross-sectional views of the samples. Images on the right refer to samples after SI-ATRP and show a polymer layer stratification on the top surface (smaller and smoother pore openings). From the cross-sectional view a polymer layer of ~60 nm on top surface can be estimated (vertical black line). The cross-sectional view also shows smooth polymeric material inside the nanowell, in contrast with the cross-sectional view of the nonfunctionalized film (left), where the rough surface of the pore wall caused by the reactive-ion-etching step during film preparation is evident.[39]

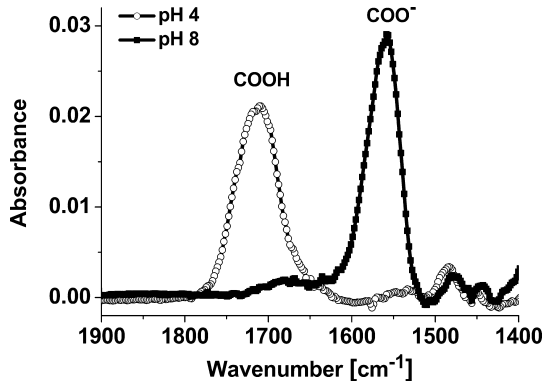

Figure 2. Carbonyl absorption region in FTIR spectra of a PMAA brush grafted from a nanoporous silicon nitride film after incubation in phosphate solution of pH 4 or pH 8. FTIR spectra display protonated PMAA chains at pH 4 and deprotonated PMAA chains at pH 8.

peak of the deprotonated carboxylic acid groups is located at 1558 cm^{-1}. These FTIR spectra prove that (i) PMAA brushes were grafted from nanoporous films and (ii) these grafts respond to pH variations.

Atomic force microscopy (AFM) characterization in liquid environment was used to follow the swell and the collapse of the PMAA brushes inside the nanopores. As displayed in the SEM images of Figure 1, the graft layers were both grown from the wall of the nanowells, as well from the top surface of the nanoporous films. The swelling of the polymer layer grafted from the top surface blocked the view at the nanopore openings by AFM. Therefore, nanoporous films with a chrome top layer were used to grow the grafts only from the silicon nitride walls of the nanowells. The chrome top layer served as a passivation layer, since there is no formation of silanol groups at the chrome surface during the activation step by piranha solution prior to the deposition of the ATRP initiator layer. It is known that chrome oxide surfaces can be functionalized by organosilanes such as trichloroalkylsilanes and triethoxyalkylsilanes.[42,43] On the other hand, there are also examples in the literature where chrome is used to create patterns where silanes do not attach, including monochlorosilanes.[44] To clarify this issue, water contact angle and XPS measurements were performed at silicon and chrome surfaces before and after vapor-phase deposition of the initiator molecules. For silicon surfaces, contact angle values before immobilization of the initiator (right after activation in piranha solution) were ~23° and increased to ~77° after initiator immobilization, indicating the presence of the hydrophobic initiator molecules on surface.[10] Chrome surfaces had a contact angle of ~13° after treatment in piranha solution, and ~17° after the deposition of the initiator molecules. These results gave a first indication that no initiator molecules were covalently linked to the chrome surface. The same silicon and chrome surfaces were investigated by XPS, and the full element analysis showed less C atoms and almost no Br atoms at the chrome surface after treatment with the ATRP initiator, as compared to the silicon surface (see Table S1 in the Supporting Information). XPS survey spectra for a silicon and chrome surface after initiator deposition are included (see Figure S1 in the Supporting Information). From both contact angle and XPS results, the conclusion was drawn that the ATRP initiator monolayer does not form on chrome surfaces when vapor-phase deposition is used. At the silicon nitride surface inside the nanowells silanol groups are formed in contact with piranha solution and therefore can be used for immobilization of monochlorosilane initiator molecules. In this way, it was possible to attach the initiator molecules only onto the silicon nitride surface and to graft polymer chains only from the nanopore walls. These PMAA-brush functionalized nanoporous films were both characterized with SEM and AFM. Using SEM, nonfunctionalized as well as functionalized nanoporous films were compared, with both the top surface and the cross section scanned in a tilted position (Figure 3). The SEM images show that the functionalized nanoporous film has polymer layers inside the nanowells. At the top surface, there is a rim of polymeric material visible at the nanopore openings. This latter observation was investigated by AFM under ambient conditions. The top surface of nonfunctionalized and PMAA-brush functionalized nanoporous films were both scanned. On the AFM images of Figure 4, it can be seen that the polymer graft protrudes out of the nanopore in the case of the functionalized silicon nitride nanoporous film, whereas there is no substance around the pore rim of the nonfunctionalized nanoporous film. Note that, away from the pore rims, the AFM images in Figure 4 show the same surface features for both the nonfunctionalized nanoporous film and the functionalized nanoporous film, and no polymer grafts attached to the chrome surface are visible. Both SEM and AFM images indicate that the passivating chrome layer method works as expected, and that there is no polymer brush grafted from the top side of the nanoporous films.

3.2. Controlled Nanopore Gating Function by pH-Responsive Poly(methacrylic acid) (PMAA) Brushes. In our previous study, in situ ellipsometry and AFM in a liquid environment were used to investigate the swell and collapse of PMAA brushes grafted from planar surfaces upon changes in the solution pH.[10] This pH-responsive behavior originates from the deprotonation of the carboxylic acids groups at higher pH values. The polymer chains become charged and repel each

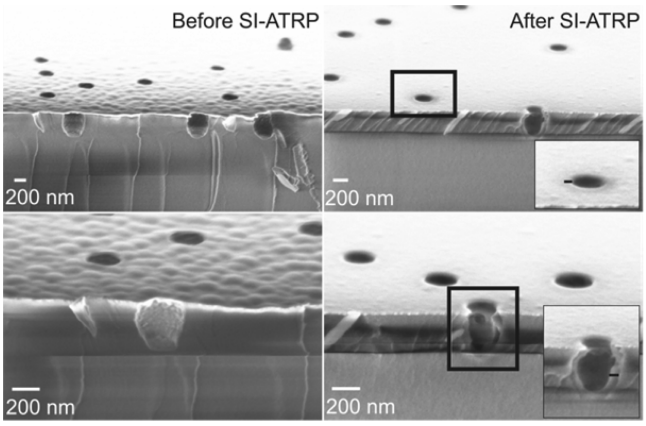

Figure 3. SEM images of non-functionalized (left) and PMAA-brush functionalized (right) nanoporous silicon nitride films with a chrome top layer. Top images display the tilted top surface and cross-sectional view together, and bottom images display an enlarged image of the cross-sectional view. Black boxes indicate polymer grafts protruding out of the pore opening (top box; also see Figure 4) and polymer layers inside the nanowell (bottom box). The insets on the right show enlarged areas of the functionalized nanowells: the horizontal black lines were added to indicate the extent of the polymer layer protruding out of the pore (top inset) and along the nanopore wall (bottom inset).

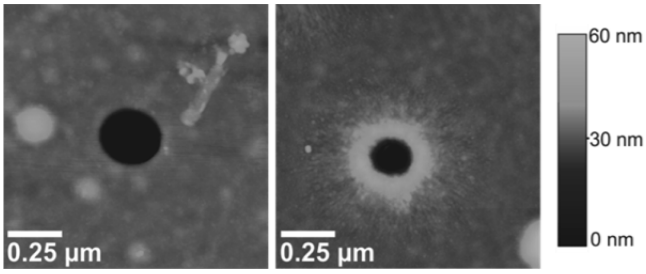

Figure 4. TM-AFM images (top view) in ambient environment of nonfunctionalized (left) and PMAA-brush functionalized (right) nanoporous silicon nitride film with a chrome top layer. In the right AFM image, polymer chains grafted from the pore wall are protruding out of the pore opening.

other, which results in swelling of the brushes. Besides the electrostatic interactions upon changes in pH, the osmotic pressure of the counterions also plays a role in the polymer-brush conformation. Large additions of salt result in the collapse of weak polyelectrolyte brushes, because of a decrease in the osmotic pressure of the counterions. Conversely, low additions of salt cause an increase in brush height via an exchange of protons for cations. This exchange produces an increase in the degree of dissociation, and, therefore, swelling of weak polyelectrolyte brushes occurs.[45] In the case of functionalized nanochannels, the pH-responsive behavior of the polymer grafts can be used as a nanopore gating function. In a previous work, we investigated brush thickness variations in phosphate solutions with pH 4 and pH 8 for PMAA grafted from planar silicon surfaces under the same conditions. Measurements by in situ ellipsometry showed large swelling in the phosphate solutions (up to ∼229 nm for pH 8) and swelling factors in the range 1.1−1.3, depending on the brush grafting density.[10] In the present situation, because of the different polymerization kinetics in the confined space of the nanopores and the accessibility of the polymer layer conformation, it is difficult to determine brush thickness variations and corresponding swelling factors. From a theoretical study, it is known that polymer chains attached close to the entrance of pores with short aspect ratios tend to protrude out of the pores in a good solvent. By protruding out of the pore into the reservoir, polymer chains relieve nanoconfinement and stretch away from the pore.[46] To observe the swelling of the PMAA grafts inside the nanowells of the nanoporous silicon nitride films, AFM measurements were performed on substrates with a passivating chrome top layer (see Figure 5). Measurements were made in a phosphate

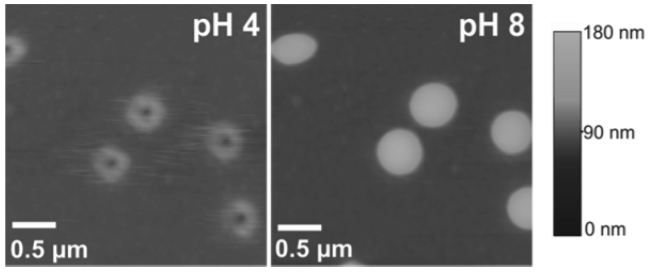

Figure 5. CM-AFM images (top view) of PMAA-brush functionalized nanoporous silicon nitride film with a chrome top layer in phosphate solution of pH 4 or pH 8. At pH 4 (left), the polymer chains protruding out of the five pore openings are swollen; nevertheless, the pore openings are not completely blocked. At pH 8 (right), there is significant swelling of the polymer chains out of the five nanowells.

solution of pH 4 (brush collapsed state) or pH 8 (maximum brush swelling in liquid). AFM characterization was also chosen to analyze the response of the PMAA brushes grafted from the nanowells in the actual environment of the application considered in this work, that is, the mechanical gating for the ion permeability control through nanopores. At both pH values, the same area with five pores with a diameter of 200 nm was scanned. A pore size of 200 nm was chosen to completely block the pores at the maximum brush swelling conformation. In fact, our previous study on PMAA brushes grafted from planar silicon surfaces had displayed a maximum brush swelling of up to ∼229 nm in phosphate solutions of pH 8.[10] Compared to the AFM image obtained under dry conditions in Figure 4, the polymer grafts in Figure 5 were already swollen by the uptake of phosphate solution. It can be seen from the corresponding AFM image taken at pH 4 that the nanopores at this pH value are not closed by the graft. After changing the liquid in the AFM liquid cell to the pH 8 phosphate solution, the same area was scanned again and a significant swelling of the PMAA brushes out of the pores was observed. This result displays the opening and closing of PMAA-brush functionalized nanopores with the chosen polymerization conditions by changing the pH of the surrounding environment from pH 4 to pH 8.

To investigate the pH-controlled gating properties of the PMAA brushes, nanopore array chips with channels accessible on both sides in a silicon nitride membrane were functionalized with SI-ATRP and analyzed in current−voltage measurements. Chips with arrays of four nanochannels with a diameter of 400 nm were used, and the ionic conductance was obtained at different pH values of the phosphate solution. Here, nanochannels 400 nm in diameter were used to limit the entrapment of air bubbles, which would affect the conductivity measurements. At each pH value, a current−voltage measurement was applied where the voltage was cycled between −0.2 V and 0.2 V

at a sweep rate of 10 mV/s and the current across the functionalized chip was measured (Figure 6). From 0 V to 0.2

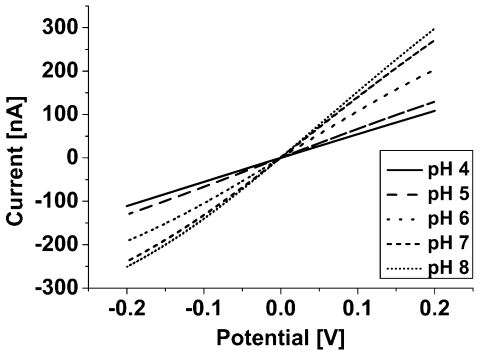

Figure 6. Current–voltage measurements of a PMAA-brush functionalized nanopore array (4 pores 400 nm in diameter) at varied pH values.

V, the $I-V$ curves for all pH values were linear and the resistance was calculated from the slopes. The graph in Figure 7

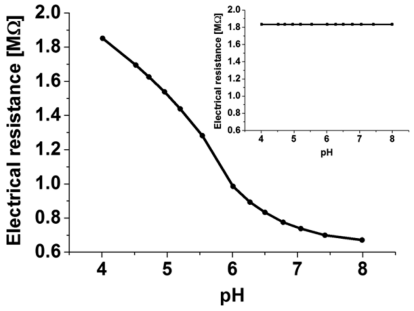

Figure 7. Change in electrical resistance of a PMAA-brush functionalized nanopore array at varied pH values. By increasing the solution pH, the electrical resistance decreases. Inset (same axes) displays control experiment with a nonfunctionalized nanopore array, which displays no response to variations of pH solution.

shows the decrease of electrical resistance with increasing pH, which implies that charging up the PMAA chains favors ion transport across the nanopore array chip. This behavior is in agreement with previous published work on nanochannels functionalized with PVP brushes, if we consider the different nature of the polymer brush and its opposite pH-dependent gating properties.[29] In that case, in fact, a significant decrease in the transmembrane ionic current was measured with increasing solution pH, that is when the PVP chains are in the neutral state. The inset in Figure 7 displays the result of a control experiment performed with a nonfunctionalized nanopore array chip with one pore with a diameter of 800 nm. The same phosphate solutions with varied pH values were used to confirm that the change in electrical resistance over the nanopore array chip is coming from the PMAA graft. The graph in the inset shows no change in electrical resistance by variation of pH. The reversibility of PMAA brushes between pH 4 and pH 8 was investigated in depth in our previous study, where the degree of dissociation by FTIR and the brush thickness by in situ ellipsometry displayed reversibility over four pH cycles.[10] In this study, the $I-V$ measurements were repeated in solution of various pH values between pH 4 and pH 8 in a cycle. Figure 7 displays the curve obtained from pH 8 to pH 4. In the Supporting Information, the complete cycle starting from pH 4 to pH 8 and back is presented (see Figure S2), which shows, for all pH values, a reproducible value in electrical resistance. These results confirm that (i) PMAA brushes are grafted from nanopore array chips and (ii) they respond to variations of pH in their environment. The ionic conductance across PMAA-brush functionalized nanochannels can be controlled by varying the pH of the surrounding environment.

Results from the AFM measurements on PMAA-grafted nanowells (Figure 5) clearly show that the pores are open at pH 4 and closed at pH 8. To further assess the mechanical gating properties of the polymer brush, in response to pH variations, fluorescent dye diffusion experiments were performed using functionalized chips with arrays having 512 pores with diameters of 800 nm. Pore diameter sizes of 800 nm were chosen to avoid bubble entrapment in the sieve, to have a reproducible diffusion area under different solution conditions. At the same time, in the permeability measurements, it was necessary to maximize the throughput of the diffusing fluorescent dye so that it could be measured by a fluorometer. A two-chamber setup filled with phosphate solution of pH 4 or pH 8 was used and the diffusion of the fluorescent dye Rhodamine 6G across the chip was followed. Samples were taken after fixed time intervals and analyzed by fluorescence spectroscopy. The intensities given by fluorescence spectroscopy were used to backcalculate the concentration of the samples with use of the calibration curves for pH 4 and pH 8. The relative concentrations of diffused Rhodamine 6G were calculated with respect to the start concentration and are shown in Table 1. From this table, it can be seen that the translocated

Table 1. Relative Concentrations of Rhodamine 6G from Diffusion Experiments with PMAA-Functionalized Nanopore Chips (Pore Diameter = 800 nm) at pH 4 and pH 8[a]

	relative concentration of diffused Rhodamine 6G [% × 10^2]
Chip 1	
pH 4 after 19.5 h	12.8
pH 8 after 19.5 h	0.73
Chip 2	
pH 8 after 16 h	1.82
pH 4 after 16 h	6.3

[a]Regardless of the order of the solution applied first, slower diffusion of Rhodamine 6G across the functionalized nanochannels is measured with solutions of pH 8.

fluorophore concentrations obtained at pH 4 are higher than those obtained at pH 8 after 19.5 h or 16 h. Changing the order in which the two phosphate solutions were applied yielded the same result. The pK_a of Rhodamine 6G must be taken into account; this value is ~7.5, which means that Rhodamine 6G is positively charged at pH 8. At pH 8, the negatively charged PMAA chains and the positively charged Rhodamine 6G molecules form ion pairs, resulting in hindered diffusion across the chips. From this, it is clear that the diffusion of Rhodamine 6G in the pore with a charged environment and more closed state at pH 8 is slower due to both brush hindrance effect and Rhodamine 6G binding to the polymer layer. These results show that mechanical gating by pH-controlled PMAA brushes grafted from nanochannels is possible. Further analysis of the permeability data, in terms of diffusion coefficients, was difficult

to perform for this system, because of the complicated geometry of the interface of the functionalized nanochannels and the confinement effect that plays an important role on the acid−base equilibrium of the pH-responsive brush.[11] A concentration gradient was used as the driving force for dye diffusion. At pH 8, the swollen brush blocks the pores more than at pH 4, resulting in hindered diffusion. In addition, the previous mentioned electrostatic interaction between Rhodamine 6G and the charged polymer chains at pH 8 further decreases the dye diffusion. As a result of both effects, nanochannels functionalized with PMAA brushes can be effectively used for stimuli-gated nanofiltration.

4. CONCLUSIONS

Nanoporous platforms were functionalized with pH-responsive poly(methacrylic acid) (PMAA) brushes using surface-initiated atom transfer radical polymerization (SI-ATRP). Polymer grafting from silicon nitride films with etched nanowells was confirmed by scanning electron microscopy (SEM) and Fourier transform infrared (FTIR) characterization. The same nanoporous films with a passivating chrome top layer were used to synthesize PMAA grafts only on the walls of the nanowells. The swell and collapse of the pH-responsive polymer chains on the pore walls was investigated by atomic force microscopy (AFM) in a liquid environment of pH 4 or pH 8. The AFM images displayed open pores at pH 4 and closed pores at pH 8.

Several nanopore gating functions of PMAA-brush functionalized nanopore array chips were explored. The gating of ions could be controlled by varying the pH of the surrounding environment of the functionalized nanochannels. Increasing the pH of the surrounding environment resulted in a decrease of electrical resistance across the nanochannels. Mechanically gating was investigated by following the diffusion of a fluorescent dye across the functionalized nanochannels. Diffusion of the dye molecule was slower at pH 8 when the PMAA chains are in a charged and swollen state, thereby hindering the diffusion through the nanochannels.

The properties of the pH-responsive PMAA-brush functionalized nanoporous platforms illustrate the potential applications in electrochemical (bio)sensors for the controlled gating of ions and in nanofluidics as valves for low-molecular-weight molecules.

■ ASSOCIATED CONTENT

Supporting Information

Characterization of silicon and chrome surfaces before and after vapor-phase deposition of the ATRP initiator molecules by XPS (Table S1 and Figure S1). Change in the electrical resistance of PMAA-brush functionalized nanopore array over a cycle between pH 4 and pH 8 (Figure S2). This material is available free of charge via the Internet at http://pubs.acs.org.

■ AUTHOR INFORMATION

Corresponding Author

*Tel.: +31-53-4892967. Fax: +31-53-4893823. E-mail: g.j.vancso@utwente.nl.

Present Addresses

[∇]Department of Chemical Engineering Materials and Environment, Sapienza University of Rome, Via Eudossiana 18, 00184 Rome, Italy.

[#]Max Planck Institute for Intelligent Systems, Heisenbergstrasse 3, 70569 Stuttgart, Germany.

Author Contributions

The manuscript was written through contributions of all authors. All authors have given approval to the final version of the manuscript.

Notes

The authors declare no competing financial interest.

■ ACKNOWLEDGMENTS

This work was financially supported by the European Commission through the FP7 program ASMENA (Grant No. CP-FP 214666-2). We thank Karthik Kumar and Mateu Pla Roca (Laboratory for Surface Science and Technology, ETH Zürich) for the preparation of nanoporous silicon nitride films, and Marco Di Berardino (Leister Technologies AG) for the nanopore chip fabrication. We are also grateful to Mark A. Smithers and Gerard Kip (MESA+ Institute for Nanotechnology, University of Twente) for technical assistance with SEM imaging and XPS measurements.

■ REFERENCES

(1) Reimhult, E.; Kumar, K. *Trends Biotechnol.* **2008**, *26*, 82−89.
(2) Stuart, M. A. C.; Huck, W. T. S.; Genzer, J.; Muller, M.; Ober, C.; Stamm, M.; Sukhorukov, G. B.; Szleifer, I.; Tsukruk, V. V.; Urban, M.; Winnik, F.; Zauscher, S.; Luzinov, I.; Minko, S. *Nat. Mater.* **2010**, *9*, 101−113.
(3) Barbey, R.; Lavanant, L.; Paripovic, D.; Schuwer, N.; Sugnaux, C.; Tugulu, S.; Klok, H. A. *Chem. Rev.* **2009**, *109*, 5437−5527.
(4) Matyjaszewski, K.; Xia, J. H. *Chem. Rev.* **2001**, *101*, 2921−2990.
(5) Luzinov, I.; Minko, S.; Tsukruk, V. V. *Soft Matter* **2008**, *4*, 714−725.
(6) Ducker, R.; Garcia, A.; Zhang, J. M.; Chen, T.; Zauscher, S. *Soft Matter* **2008**, *4*, 1774−1786.
(7) Nagase, K.; Kimura, A.; Shimizu, T.; Matsuura, K.; Yamato, M.; Takeda, N.; Okano, T. *J. Mater. Chem.* **2012**, *22*, 19514−19522.
(8) Adiga, S. P.; Brenner, D. W. *J. Funct. Biomater.* **2012**, *3*, 239−256.
(9) Tagliazucchi, M.; Azzaroni, O.; Szleifer, I. *J. Am. Chem. Soc.* **2010**, *132*, 12404−12411.
(10) Santonicola, M. G.; de Groot, G. W.; Memesa, M.; Meszynska, A.; Vancso, G. J. *Langmuir* **2010**, *26*, 17513−17519.
(11) Tagliazucchi, M.; Szleifer, I. *Soft Matter* **2012**, *8*, 3292−3305.
(12) Sugihara, K.; Voros, J.; Zambelli, T. *ACS Nano* **2010**, *4*, 5047−5054.
(13) Kumar, K.; Isa, L.; Egner, A.; Schmidt, R.; Textor, M.; Reimhult, E. *Langmuir* **2011**, *27*, 10920−10928.
(14) Simonsson, L.; Gunnarsson, A.; Wallin, P.; Jonsson, P.; Hook, F. *J. Am. Chem. Soc.* **2011**, *133*, 14027−14032.
(15) Roder, F.; Waichman, S.; Paterok, D.; Schubert, R.; Richter, C.; Liedberg, B.; Piehler, J. *Anal. Chem.* **2011**, *83*, 6792−6799.
(16) Lazzara, T. D.; Kliesch, T. T.; Janshoff, A.; Steinem, C. *ACS Appl. Mater. Interfaces* **2011**, *3*, 1068−1076.
(17) Santonicola, M. G.; Memesa, M.; Meszynska, A.; Ma, Y. J.; Vancso, G. J. *Soft Matter* **2012**, *8*, 1556−1562.
(18) Overington, J. P.; Al-Lazikani, B.; Hopkins, A. L. *Nat. Rev. Drug Discovery* **2006**, *5*, 993−996.
(19) Arinaminpathy, Y.; Khurana, E.; Engelman, D. M.; Gerstein, M. B. *Drug Discovery Today* **2009**, *14*, 1130−1135.
(20) Dai, J. H.; Bao, Z. Y.; Sun, L.; Hong, S. U.; Baker, G. L.; Bruening, M. L. *Langmuir* **2006**, *22*, 4274−4281.
(21) Sun, L.; Dai, J. H.; Baker, G. L.; Bruening, M. L. *Chem. Mater.* **2006**, *18*, 4033−4039.
(22) Tang, M.; Zhang, R.; Bowyer, A.; Eisenthal, R.; Hubble, J. *Biotechnol. Bioeng.* **2003**, *82*, 47−53.
(23) Bernstein, R.; Anton, E.; Ulbricht, M. *ACS Appl. Mater. Interfaces* **2012**, *4*, 3438−3446.
(24) Ito, Y.; Inaba, M.; Chung, D. J.; Imanishi, Y. *Macromolecules* **1992**, *25*, 7313−7316.
(25) Ito, Y.; Park, Y. S.; Imanishi, Y. *Langmuir* **2000**, *16*, 5376−5381.

(26) Zhang, H. J.; Ito, Y. *Langmuir* **2001**, *17*, 8336−8340.
(27) Alem, H.; Duwez, A. S.; Lussis, P.; Lipnik, P.; Jonas, A. M.; Demoustier-Champagne, S. *J. Membr. Sci.* **2008**, *308*, 75−86.
(28) Alem, H.; Jonas, A. M.; Demoustier-Champagne, S. *Polym. Degrad. Stab.* **2010**, *95*, 327−331.
(29) Yameen, B.; Ali, M.; Neumann, R.; Ensinger, W.; Knoll, W.; Azzaroni, O. *Nano Lett.* **2009**, *9*, 2788−2793.
(30) Yameen, B.; Kaltbeitzel, A.; Langner, A.; Duran, H.; Muller, F.; Gosele, U.; Azzaroni, O.; Knoll, W. *J. Am. Chem. Soc.* **2008**, *130*, 13140−13144.
(31) Yameen, B.; Kaltbeitzel, A.; Glasser, G.; Langner, A.; Muller, F.; Gosele, U.; Knoll, W.; Azzaroni, O. *ACS Appl. Mater. Interfaces* **2010**, *2*, 279−287.
(32) Sugihara, K.; Voros, J.; Zambelli, T. *J. Phys. Chem. B* **2010**, *114*, 13982−13987.
(33) Lin, Y. H.; Teng, J.; Zubarev, E. R.; Shulha, H.; Tsukruk, V. V. *Nano Lett.* **2005**, *5*, 491−495.
(34) Benetti, E. M.; Reimhult, E.; de Bruin, J.; Zapotoczny, S.; Textor, M.; Vancso, G. J. *Macromolecules* **2009**, *42*, 1640−1647.
(35) Sui, X. F.; Zapotoczny, S.; Benetti, E. M.; Schon, P.; Vancso, G. J. *J. Mater. Chem.* **2010**, *20*, 4981−4993.
(36) Kutnyanszky, E.; Vancso, G. J. *Eur. Polym. J.* **2012**, *48*, 8−15.
(37) Lim, R. Y. H.; Deng, J. *ACS Nano* **2009**, *3*, 2911−2918.
(38) Jovanovic-Talisman, T.; Tetenbaum-Novatt, J.; McKenney, A. S.; Zilman, A.; Peters, R.; Rout, M. P.; Chait, B. T. *Nature* **2009**, *457*, 1023−1027.
(39) Reimhult, E.; Kumar, K.; Knoll, W. *Nanotechnology* **2007**, *18*, 275303.
(40) Isa, L.; Kumar, K.; Muller, M.; Grolig, J.; Textor, M.; Reimhult, E. *ACS Nano* **2010**, *4*, 5665−5670.
(41) Heyderman, L. J.; Ketterer, B.; Bachle, D.; Glaus, F.; Haas, B.; Schift, H.; Vogelsang, K.; Gobrecht, J.; Tiefenauer, L.; Dubochet, O.; Surbled, P.; Hessler, T. *Microelectron. Eng.* **2003**, *67-8*, 208−213.
(42) Anac, I.; McCarthy, T. J. *J. Colloid Interface Sci.* **2009**, *331*, 138−142.
(43) Hild, R.; David, C.; Muller, H. U.; Volkel, B.; Kayser, D. R.; Grunze, M. *Langmuir* **1998**, *14*, 342−346.
(44) Fujihira, M.; Morita, Y. *J. Vac. Sci. Technol. B* **1994**, *12*, 1609−1613.
(45) Biesalski, M.; Johannsmann, D.; Ruhe, J. *J. Chem. Phys.* **2002**, *117*, 4988−4994.
(46) Peleg, O.; Tagliazucchi, M.; Kroger, M.; Rabin, Y.; Szleifer, I. *ACS Nano* **2011**, *5*, 4737−4747.